STRUCTURAL CONTROL AND HEALTH MONITORING
Struct. Control Health Monit. 2006; **13**:589–604
Published online 24 November 2005 in Wiley InterScience (www.interscience.wiley.com). DOI: 10.1002/stc.100

Smart base-isolated benchmark building. Part II: phase I sample controllers for linear isolation systems

S. Nagarajaiah[1,*,†] and S. Narasimhan[2]

[1] *Department of Civil and Environmental Engineering and Mechanical Engineering and Materials Science, Rice University, Houston, TX 77005, U.S.A.*
[2] *Department of Civil and Environmental Engineering, Rice University, Houston, TX 77005, U.S.A.*

SUMMARY

Sample controllers for a three-dimensional smart base-isolated building benchmark problem with linear and frictional isolation system are presented in this paper. A Kalman filter is used to estimate the states based on absolute acceleration measurements. Input filters are used to better inform the controller of the spectral content of the earthquake excitations. A reduced order control-oriented model of the benchmark structure with a linear isolation system is developed. A H_2/linear quadratic Gaussian controller is presented for the active case; additionally, a clipped optimal controller is presented for the semiactive case. A preliminary 'skyhook' semiactive controller is also presented for the benchmark problem. Magnetorheological fluid dampers are used for control in the semiactive case and ideal actuators are used for control in the active case. The focus of this phase I study is on the linear isolation system only. Computed results for the passive, semiactive, and active cases are presented. Detailed comparisons of benchmark performance indices for base-isolated structures with a nominal linear isolation system, with and without control, for a set of strong near-field earthquakes are presented. The modeling and sample control designs demonstrated in this paper can be used to form the basis for studying a wide variety of active and semiactive control strategies—to be developed by the participants in the benchmark study—for linear base-isolated buildings. Copyright © 2005 John Wiley & Sons, Ltd.

KEY WORDS: benchmark problem; smart base-isolated building; active; semiactive; H_2/LQG; skyhook; seismic response control

1. INTRODUCTION

Several researchers have studied passive, active and semiactive control of base-isolated structures [1–15,37,43]. However, the relative merits of these active and semiactive controllers,

*Correspondence to: Associate Professor S. Nagarajaiah, Department of Civil and Environmental Engineering and Mechanical Engineering and Materials Science, Rice University, Houston, TX 77005, U.S.A.
† E-mail: nagaraja@rice.edu

Contract/grant sponsor: National Science Foundation; contract/grant number: 9996290

Received 9 September 2004
Revised 1 December 2004
Accepted 15 December 2004

as applied to base-isolated structures, has not been investigated by careful comparison on a well-defined benchmark problem. Recently well-defined analytical benchmark problems [16–21] have been developed for studying response control strategies for building and bridge structures subjected to seismic and wind excitation, by broad consensus effort of the ASCE structural control committee. The goal of this effort was to develop benchmark models to provide systematic and standardized means by which competing control strategies, including devices, algorithms, sensors, etc. can be evaluated. Carefully defined analytical benchmark problems are an excellent alternative to expensive experimental benchmark test structures. Due to the effectiveness of the fixed-base building benchmark effort [17–20] the ASCE structural control committee voted to develop a new smart base-isolated benchmark problem. Narasimhan *et al.* [22–25] and Nagarajaiah *et al.* [26, 27] have developed the smart base-isolated benchmark problem, based on input from the ASCE structural control committee, with the capability to model different kinds of base isolation systems [39–41]: linear elastomeric systems with low damping or supplemental high damping; frictional systems; bilinear or nonlinear elastomeric systems or any combination thereof. The superstructure is assumed to remain linear at all times. A host of control devices can be considered at the isolation level. No control devices are allowed in the superstructure.

This paper presents sample control strategies for benchmark problem with nominal linear isolation systems. Actuators are used for active control or magnetorheological (MR) dampers are used for semiactive control. To illustrate some of the design challenges active and semiactive control algorithms are presented for the case with linear elastomeric isolation system. Also, semiactive control algorithms with MR dampers are presented for the nonlinear friction isolation system. The presented active and semiactive sample control strategies are not meant to be competitive, but are intended to serve as guide to the participants of the benchmark study. In phase I, the participants can compare the results of their controllers with the results of the sample active and semiactive controllers presented in this paper for the nominal linear isolation system. Additionally, they may also compare the results of their controllers with a preliminary skyhook controller presented.

An H_2/LQG sample controller is presented to illustrate the implementation of the active control system in the linear isolation case. In order to illustrate the implementation of semiactive control systems in the linear isolation case, a clipped optimal controller [28] based on H_2/LQG methods is presented. A Skyhook controller [29] is also presented.

For the H_2/LQG-active and clipped optimal control designs [30], sensors placed on the eighth floor and at the isolation level measure the acceleration responses of two translational (EW and NS) and one rotational direction. In the case of skyhook control, sensors (accelerometers) are placed at each of the control device locations, a total of eight in the EW and NS directions, respectively, and a sensor to measure ground acceleration.

The H_2/LQG design is based on a reduced order model [31] that contains 24 states compared with 54 states in the full-order model. The frequency characteristics of the ground excitation are incorporated into the control design through a shaping filter. The resulting H_2/LQG controller is designed for the augmented system consisting of 28 states. The skyhook control case uses both the relative and absolute velocities at the measured locations. These velocities are computed from acceleration measurements through the use of a higher-order filter that approximates an integrator.

2. NOMINAL LINEAR ELASTOMERIC ISOLATION SYSTEM

The nominal linear isolation system consists of 92 low-damping elastomeric bearings. The fundamental period, T_b is 3 s in the linear elastomeric isolation case. The damping in the linear elastomeric isolation system is considered to be 3% of critical. The second isolation system considered consists of 92 linear elastomeric bearings with 61 passive friction dampers. The fundamental period, T_b is 3 s in the second isolation case also. A coefficient of friction $\mu = 0.06$ is considered for the friction dampers. In all cases total of 16 active or semiactive control devices, 8 in the X and 8 in the Y direction, are placed at the isolation level.

3. ACTIVE CONTROL: LINEAR ELASTOMERIC ISOLATION SYSTEM

The state equation [24, 25] is as follows

$$\dot{\mathbf{X}}(t) = \mathbf{A}\mathbf{X}(t) + \mathbf{B}\mathbf{u}(t) + \mathbf{E}\ddot{\mathbf{U}}_g(t) = \mathbf{g}(\mathbf{X}, \mathbf{u}, \ddot{\mathbf{U}}_g) \tag{1}$$

where $\mathbf{X} = \{\mathbf{U}^T \ \mathbf{U}_b^T \ \dot{\mathbf{U}}^T \ \dot{\mathbf{U}}_b^T\}^T$

$$\mathbf{A} = \begin{bmatrix} \mathbf{0} & \mathbf{I} \\ -\overline{\mathbf{M}}^{-1}\overline{\mathbf{K}} & -\overline{\mathbf{M}}^{-1}\overline{\mathbf{C}} \end{bmatrix}, \quad \mathbf{B} = \mathbf{B}^* = \begin{bmatrix} \mathbf{0} \\ -\overline{\mathbf{M}}^{-1}\begin{Bmatrix} \mathbf{0} \\ \mathbf{I} \end{Bmatrix} \end{bmatrix} \tag{2}$$

$$\mathbf{E} = \begin{bmatrix} \mathbf{0} \\ -\overline{\mathbf{M}}^{-1}\begin{Bmatrix} \mathbf{MR} \\ \mathbf{R}^T\mathbf{MR} + \mathbf{M}_b \end{Bmatrix} \end{bmatrix}$$

$$\overline{\mathbf{M}} = \begin{bmatrix} \mathbf{M}_{n\times n} & \mathbf{M}_{n\times n}\mathbf{R}_{n\times 3} \\ \mathbf{R}_{3\times n}^T\mathbf{M}_{n\times n} & \mathbf{R}_{3\times n}^T\mathbf{M}_{n\times n}\mathbf{R}_{n\times 3} + \mathbf{M}_{3\times 3} \end{bmatrix}, \quad \overline{\mathbf{C}} = \begin{bmatrix} \mathbf{C}_{n\times n} & \mathbf{0} \\ \mathbf{0} & \mathbf{C}_{b_{3\times 3}} \end{bmatrix}$$

$$\overline{\mathbf{K}} = \begin{bmatrix} \mathbf{K}_{n\times n} & \mathbf{0} \\ \mathbf{0} & \mathbf{K}_{b_{3\times 3}} \end{bmatrix}, \quad \mathbf{u} = \begin{bmatrix} \mathbf{0} \\ \mathbf{f}_{c_{3\times 1}} \end{bmatrix} \tag{3}$$

In these equations, $\mathbf{A}$, $\mathbf{B}$, $\mathbf{B}^*$ and $\mathbf{E}$ are condensed system matrices having 54 states derived from the full three-dimensional finite element model. $\mathbf{M}$ is the superstructure mass matrix, $\mathbf{C}$ is the superstructure damping matrix in the fixed base case, $\mathbf{K}$ is the superstructure stiffness matrix in the fixed-base case, $\mathbf{M}_b$ is the mass matrix of the rigid base, $\mathbf{C}_b$ is the resultant damping matrix of viscous isolation elements, $\mathbf{K}_b$ is the resultant stiffness matrix of the elastic isolation elements and $\mathbf{f}_c$ is the vector containing control forces. $\mathbf{R}$ is the matrix of earthquake influence coefficients, i.e. the matrix of displacements and rotation at the center of mass of the floors resulting from a unit translation in the X and Y directions and unit rotation at the center of mass of the base. Furthermore, $\ddot{\mathbf{U}}$, $\dot{\mathbf{U}}$ and $\mathbf{U}$ represent the floor acceleration, velocity and

displacement vectors relative to the base, $\ddot{\mathbf{U}}_b$ is the vector of base acceleration relative to the ground and $\ddot{\mathbf{U}}_g$ is the vector of ground accelerations. Note $\mathbf{B}^*\mathbf{F}_B$ in Equation (8) in the previous paper in the special issue (Part I) is zero since the forces from the isolation system are accounted for by the linear isolation global stiffness and damping terms in the $\mathbf{A}$ matrix.

For controller design, this model is further reduced to 24 states using model reduction techniques [31] as compared with 54 states in a full-order model. The retained states correspond to the displacement and velocity on the eighth floor, fifth floor, first floor and base. The reduction is accomplished by constructing a matrix of lower order that has the same dominant eigenvalues and eigenvectors as the original system [31]. The state space equations can be formulated as

$$\dot{\mathbf{x}}_r = \mathbf{A}_r\mathbf{x}_r + \mathbf{B}_r\mathbf{u} + \mathbf{E}_r\ddot{\mathbf{U}}_g \tag{4}$$

$$\mathbf{z}_r = \mathbf{C}_{zr}\mathbf{x}_r + \mathbf{D}_{zr}\mathbf{u} + \mathbf{F}_{zr}\ddot{\mathbf{U}}_g \tag{5}$$

$$\mathbf{y}_{mr} = \mathbf{C}_{mr}\mathbf{x}_r + \mathbf{D}_{mr}\mathbf{u} + \mathbf{F}_{mr}\ddot{\mathbf{U}}_g + \mathbf{v}_r \tag{6}$$

where $\mathbf{A}_r$, $\mathbf{B}_r$ and $\mathbf{E}_r$ are the system matrices, $\mathbf{z}_r$ is the regulated output vector which is obtained by choosing the appropriate mapping matrices, $\mathbf{C}_{zr}$, $\mathbf{D}_{zr}$ and $\mathbf{F}_{zr}$. $\mathbf{y}_{mr}$ is the measurement vector obtained by choosing matrices $\mathbf{C}_{mr}$, $\mathbf{D}_{mr}$ and $\mathbf{F}_{mr}$ appropriately. $\mathbf{v}_r$ is the measurement noise vector. The measured outputs are the responses of the eighth floor, base and ground denoted by $\mathbf{y}_{mr} = [\ddot{\mathbf{x}}_{8ax}\ \ddot{\mathbf{x}}_{8ay}\ \ddot{\mathbf{x}}_{8a\theta}\ \ddot{\mathbf{x}}_{bax}\ \ddot{\mathbf{x}}_{bay}\ \ddot{\mathbf{x}}_{ba\theta}\ \ddot{\mathbf{u}}_{gx}\ \ddot{\mathbf{u}}_{gy}]^T$ and the outputs to be regulated include the inter-storey drifts and base displacements at the farthest corner of the building and absolute accelerations for all degrees of freedom given by $\mathbf{z}_r = [\mathbf{x}_b\ \mathbf{x}_i - \mathbf{x}_{i-1}\ \ddot{\mathbf{x}}_b\ \ddot{\mathbf{x}}_i]^T$; where, i denotes the floor under consideration.

To better inform the controller of the frequency characteristics of earthquakes, the input excitation is modeled as a filtered white noise. The shaping filter is given by

$$\begin{aligned} \dot{\mathbf{x}}_f &= \mathbf{A}_f\mathbf{x}_f + \mathbf{B}_f\mathbf{w} \\ \ddot{\mathbf{U}}_g^f &= \mathbf{C}_f\mathbf{x}_f \end{aligned} \tag{7}$$

where $\mathbf{w}$ is the white noise excitation and $\mathbf{x}_f$ are the states of the shaping filter. Combining Equation (7) with Equation (4), the augmented system becomes

$$\begin{bmatrix} \dot{\mathbf{x}}_r \\ \dot{\mathbf{x}}_f \end{bmatrix} = \begin{bmatrix} \mathbf{A}_r & \mathbf{E}_r\mathbf{C}_f \\ \mathbf{0} & \mathbf{A}_f \end{bmatrix} \begin{bmatrix} \mathbf{x}_r \\ \mathbf{x}_f \end{bmatrix} + \begin{bmatrix} \mathbf{B}_r \\ \mathbf{0} \end{bmatrix} \mathbf{u} + \begin{bmatrix} \mathbf{0} \\ \mathbf{B}_f \end{bmatrix} \mathbf{w} \tag{8}$$

from which the augmented equations can be written as

$$\dot{\mathbf{x}}_a = \mathbf{A}_a\mathbf{x}_a + \mathbf{B}_a\mathbf{u} + \mathbf{E}_a\mathbf{w} \tag{9}$$

$$\mathbf{y}_a = \mathbf{C}_{ya}\mathbf{x}_a + \mathbf{D}_{ya}\mathbf{u} + \mathbf{F}_{ya}\ddot{\mathbf{U}}_g^f + \mathbf{v}_a \tag{10}$$

$$\mathbf{z}_a = \mathbf{C}_{za}\mathbf{x}_a + \mathbf{D}_{za}\mathbf{u} + \mathbf{F}_{za}\ddot{\mathbf{U}}_g^f \tag{11}$$

where the matrices $\mathbf{A}_a$, $\mathbf{B}_a$ and $\mathbf{E}_a$ are augmented system matrices. $\mathbf{C}_{ya}$, $\mathbf{D}_{ya}$, $\mathbf{F}_{ya}$, $\mathbf{C}_{za}$, $\mathbf{D}_{za}$ and $\mathbf{F}_{za}$ are mapping matrices of appropriate dimensions. $\mathbf{v}_a$ is the measurement noise vector. As shown in Figure 1, the new shaping filter (Equation (12)), obtained by a least-squares fit, closely models

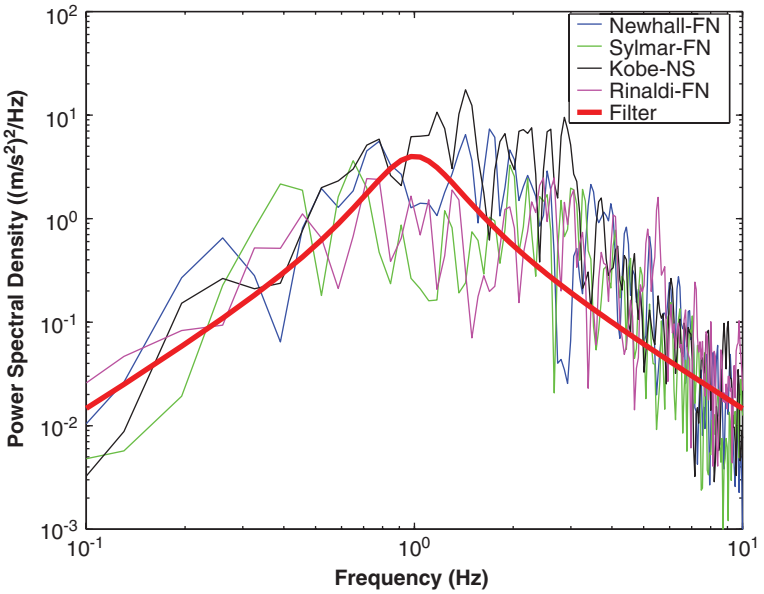

Figure 1. Excitation filter and power spectral density of earthquakes.

the ground excitation characteristics of the set of earthquakes chosen for this benchmark study, as shown in Figure 1. Other filter models such as the input shaping filter by Yoshioka *et al*. [30], or the pulse filter developed by Agrawal and Xu [32] may also be used to model ground excitation. The new shaping filter is as follows:

$$F(s) = \frac{4\zeta_g \omega_g s}{s^2 + 2\zeta_g \omega_g s + \omega_g^2}, \qquad \text{where} \qquad \omega_g = 2\pi \text{ rad/s} \qquad \zeta_g = 0.3 \tag{12}$$

The measured responses contain identically distributed RMS noise of 0.14 V and they are modelled as Gaussian rectangular pulse processes with a pulse width of 0.005 s. The sensor gains are given by $(10/9.81)[\mathbf{I}]\text{V}/(\text{m/s}^2)$, where $\mathbf{I}$ is of order 8. Assuming the independence of ground excitation and measurement noises, a cost function that weights the regulated outputs and the control forces is given as

$$J = \lim_{\tau \to \infty} \frac{1}{\tau} E\left[\int_0^\tau (\mathbf{z}_a^{\mathrm{T}} \mathbf{Q} \mathbf{z}_a + \mathbf{u}^{\mathrm{T}} \mathbf{R} \mathbf{u})\, \mathrm{d}t\right] \tag{13}$$

where $\mathbf{R}$ is an identity matrix that weights the control forces and $\mathbf{Q}$ is a diagonal matrix of the form $10^3 \times \mathbf{I}_{54\times 54}$ that weights the regulated outputs. The separation principle allows the control and estimation problems to be treated independently (for linear systems only). The control law takes the form

$$\mathbf{u} = -\mathbf{K}_a \hat{\mathbf{x}}_a \tag{14}$$

where, $\mathbf{K}_a$ is the full state feedback gain matrix and $\hat{\mathbf{x}}_a$ is the Kalman filter [42] estimate of the state vector based on the augmented model. The block diagram for the augmented controller is shown in Figure 2.

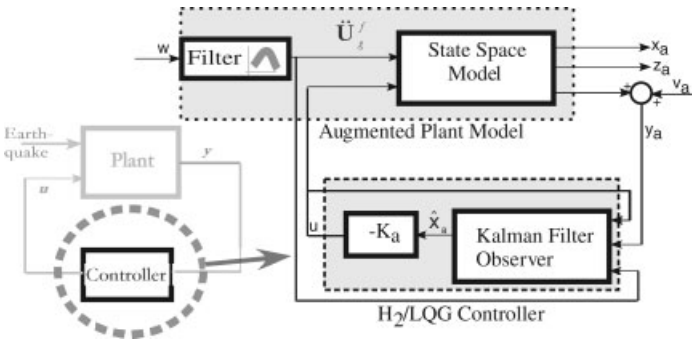

Figure 2. Design of H_2/LQG controller.

Calculations of $\mathbf{K}_a$ and the Kalman estimator gains are performed using MATLAB [38] control toolbox functions *lqry* and *lqe2*. Calculations to determine the discrete time compensator are performed using the function *c2dm* in MATLAB [38]. The state space and output matrices, $\mathbf{A}_{cd}$, $\mathbf{B}_{cd}$, $\mathbf{C}_{cd}$ and $\mathbf{D}_{cd}$ generated by *c2dm* are used in the controller block in Figures 6 and 8 of Part I [25].

4. SEMIACTIVE CONTROL: LINEAR ELASTOMERIC ISOLATION SYSTEM

In order to illustrate the application of semiactive control system using MR dampers [33, 34], a clipped optimal control strategy [28] based on H_2/LQG method is presented. The clipped optimal control approach involves the design of a controller for an active system with the desired optimal control force being generated by an MR damper according to the voltage control law,

$$u = V_{\max} H(\{f_c - f_{MR}\} f_{MR}) \tag{15}$$

where $V_{\max}$ is the maximum voltage, H is the heaviside function, f_c is the optimal force required as per Equation (14) and f_{MR} is the force that is generated by the MR damper. For better performance, the control signal generated by the digital controller is passed through a low-pass filter before it is commanded to the device. The filter is given by

$$\dot{v} = -\zeta v + \zeta u \tag{16}$$

where, the filter parameter, $\zeta = 10$ rad/s. The force generated by the damper is a function of the voltage supplied. The damper is modeled using a spring, a dashpot and hysteretic element in parallel, as shown in Figure 3. The force generated by the damper is given by

$$f_{MR} = (\alpha z) f(v) + C\dot{U}_b + kU_b \tag{17}$$

where, $\alpha(v) = \alpha_a + \alpha_b$, $C(v) = C_a + C_b$, $f(v)$ is a function of the voltage v, supplied to the MR damper. The hysteresis variable z is obtained by solving the differential equation:

$$Y_i \dot{z}_i + \gamma |\dot{U}_{bi}| z_i |z_i| + \beta \dot{U}_{bi} z_i^2 - \dot{U}_{bi} = 0 \tag{18}$$

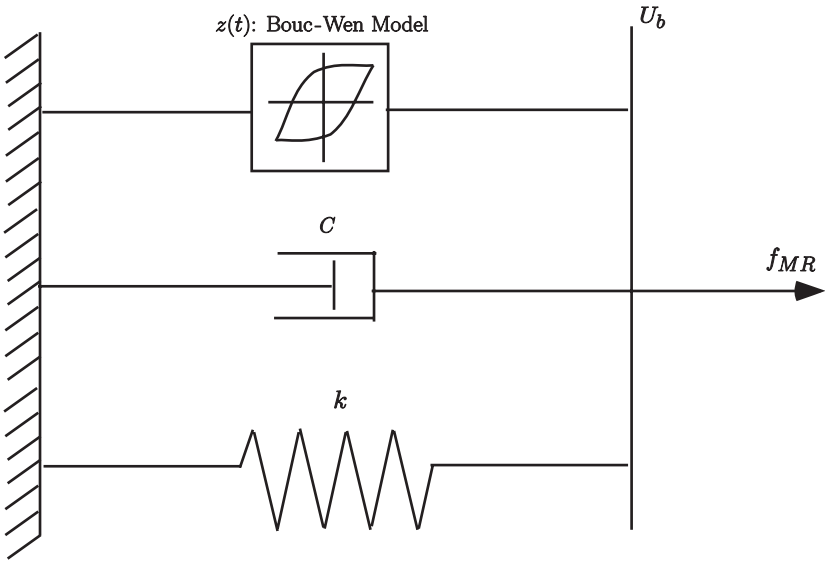

Figure 3. MR damper model.

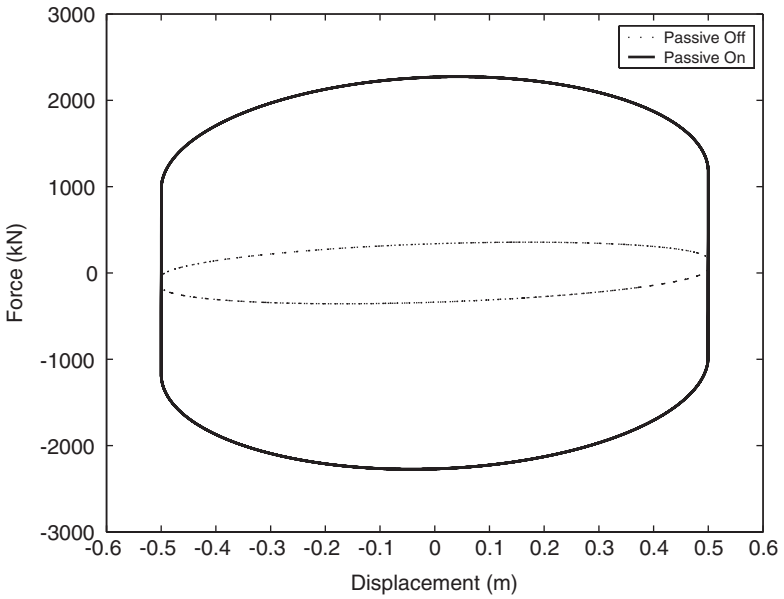

Figure 4. Force–displacement of MR damper.

where U_b is the displacement experienced by the MR damper. The parameter Y_i is the yield displacement of the hysteretic element, γ, β, α_a, α_b, C_a and C_b are constants. The force displacement characteristics of one of the eight MR dampers subjected to harmonic excitation is shown in Figure 4 for both passive-on and passive-off cases.

5. SKYHOOK CONTROL: LINEAR ISOLATION WITH FRICTION

A preliminary skyhook controller [29] is used to illustrate the semiactive control strategy for the second linear isolation case with friction dampers. The skyhook control algorithm is given by

$$C(t) = \begin{cases} C_{\max}\dot{u}_b & \dot{u}_a\dot{u}_b > 0 \\ C_{\min}\dot{u}_b & \dot{u}_a\dot{u}_b < 0 \end{cases} \tag{19}$$

Here, $C_{\min}$ is the minimum damping coefficient, $C_{\max}$ is the maximum damping coefficient of the damper, $\dot{u}_a$ is the absolute velocity and $\dot{u}_b$ is the relative velocity. The velocities are computed from acceleration measurements at the eight device locations through the use of a second-order filter [17] which approximates an integrator. The measured outputs at the eight MR damper locations are represented as $\mathbf{y}_{mf} = [\ddot{x}_{dev1}\ \ddot{x}_{dev2}\ \ddot{x}_{dev3}\ \ddot{x}_{dev4}\ \ddot{x}_{dev5}\ \ddot{x}_{dev6}\ \ddot{x}_{dev7}\ \ddot{x}_{dev8}]^T$. Notice that the measured outputs in the nominal linear elastomeric isolation system and the linear isolation with friction are not the same. Participants may choose any realistic set of measurements that is possible with the currently available technology for designing their control strategy.

6. EVALUATION OF SAMPLE CONTROL DESIGNS

The results of the evaluations for three different control designs are presented in Tables I–XI. The results presented in Tables I–VI are for the fault normal (FN) component and the fault parallel (FP) components acting in two perpendicular directions; the evaluation is reported in

Table I. Results for active control (FP-x and FN-y).

Earthquake	J1	J2	J3	J4	J5	J6	J7	J8	J9
Newhall	0.86	0.88	0.80	0.84	0.87	0.14	0.68	0.79	0.44
Sylmar	0.93	0.94	0.93	0.95	0.95	0.13	0.72	0.84	0.45
El Centro	0.97	0.95	0.83	0.81	0.82	0.10	0.78	0.70	0.37
Rinaldi	0.97	0.96	0.95	0.94	0.97	0.13	0.73	0.74	0.46
Kobe	0.84	0.85	0.79	0.82	0.90	0.10	0.75	0.69	0.41
Jiji	0.90	0.89	0.85	0.89	0.90	0.09	0.81	0.87	0.34
Erzinkan	0.99	1.02	0.79	0.85	0.99	0.11	0.80	0.78	0.45

Table II. Results for active control (FN-x and FP-y).

Earthquake	J1	J2	J3	J4	J5	J6	J7	J8	J9
Newhall	0.80	0.86	0.75	0.85	0.84	0.15	0.72	0.72	0.43
Sylmar	0.96	0.94	0.91	0.92	0.92	0.13	0.71	0.73	0.54
El Centro	0.99	0.98	0.93	0.97	1.02	0.09	0.80	0.77	0.37
Rinaldi	0.90	0.94	0.74	0.95	0.94	0.10	0.67	0.63	0.48
Kobe	0.98	0.98	0.83	0.96	0.94	0.10	0.87	0.79	0.27
Jiji	0.86	0.85	0.79	0.84	0.84	0.12	0.78	0.75	0.41
Erzinkan	0.90	0.90	0.74	0.91	0.92	0.12	0.73	0.71	0.52

Table III. Results for clipped optimal control (FP-x and FN-y).

Earthquake	Case	J1	J2	J3	J4	J5	J6	J7	J8	J9
Newhall	Passive	0.91	0.95	0.51	1.30	2.49	0.34	0.25	1.07	0.89
	control	0.97	1.02	0.56	1.04	1.49	0.30	0.33	0.89	0.79
Sylmar	Passive	0.90	0.93	0.66	0.81	1.48	0.25	0.40	0.82	0.86
	control	0.90	0.91	0.73	0.87	1.16	0.24	0.45	0.74	0.81
El Centro	Passive	0.73	0.87	0.14	1.22	2.86	0.67	0.09	1.61	0.82
	control	1.25	1.24	0.54	1.26	1.61	0.38	0.42	0.76	0.65
Rinaldi	Passive	0.95	0.96	0.50	0.97	1.12	0.29	0.27	0.83	0.86
	control	1.04	1.02	0.60	0.96	1.01	0.27	0.38	0.71	0.77
Kobe	Passive	0.84	0.84	0.36	1.19	2.34	0.39	0.16	1.14	0.87
	control	1.04	1.03	0.52	1.00	1.63	0.28	0.26	0.73	0.73
Jiji	Passive	0.83	0.82	0.65	0.86	0.92	0.17	0.42	0.82	0.70
	control	0.84	0.84	0.65	0.86	0.87	0.17	0.46	0.72	0.64
Erzinkan	Passive	0.94	0.95	0.49	0.85	1.21	0.26	0.32	0.60	0.87
	control	0.93	0.93	0.47	0.86	1.23	0.25	0.34	0.63	0.80

Table IV. Results for clipped optimal control (FP-y and FN-x).

Earthquake	Case	J1	J2	J3	J4	J5	J6	J7	J8	J9
Newhall	Passive	0.83	0.93	0.51	1.32	1.85	0.33	0.34	1.05	0.89
	control	0.88	0.92	0.55	1.24	1.40	0.30	0.42	0.84	0.80
Sylmar	Passive	0.79	0.78	0.68	0.80	1.25	0.25	0.46	0.67	0.85
	control	0.80	0.79	0.74	0.79	0.92	0.23	0.51	0.61	0.81
El Centro	Passive	0.73	0.93	0.19	2.18	3.45	0.69	0.12	2.00	0.81
	control	1.25	1.24	0.65	1.37	2.08	0.37	0.42	0.92	0.69
Rinaldi	Passive	0.88	0.93	0.53	0.93	1.12	0.28	0.24	0.58	0.87
	control	0.98	1.01	0.62	0.99	1.02	0.26	0.30	0.47	0.78
Kobe	Passive	0.96	1.00	0.40	1.30	2.24	0.41	0.20	1.44	0.87
	control	1.15	1.20	0.52	1.33	1.47	0.30	0.38	0.98	0.72
Jiji	Passive	0.74	0.74	0.63	0.75	0.77	0.17	0.40	0.74	0.70
	control	0.74	0.73	0.63	0.73	0.80	0.17	0.46	0.61	0.64
Erzinkan	Passive	0.85	0.85	0.51	0.95	1.13	0.25	0.29	0.48	0.87
	control	0.84	0.83	0.50	0.89	1.14	0.24	0.32	0.52	0.79

terms of the performance indices described in the definition paper [23–25]. The uncontrolled response quantities are presented in Tables VIII–XI for the fault normal (FN) component and the fault parallel (FP) component acting in two perpendicular directions. The term 'uncontrolled' in the following discussion refers to the isolation system containing linear and nonlinear bearings, but with no supplemental passive dampers or control devices. Time history responses in the NS direction for Newhall earthquake FN and FP components acting on the benchmark building are shown in Figure 5. The force displacement loops for the MR damper and the isolation bearings (linear and frictional) for both clipped optimal and skyhook control is shown in Figure 6. The maximum corner drifts normalized by their corresponding uncontrolled values are shown in Table VII for the three different control designs.

Table V. Results for skyhook control (FP-x and FN-y).

Earthquake		J1	J2	J3	J4	J5	J6	J7	J8	J9
Newhall	Passive	1.04	1.06	0.67	1.37	1.22	0.32	0.60	1.46	0.52
	control	0.86	0.87	0.75	1.18	1.13	0.34	0.66	1.35	0.42
Sylmar	Passive	0.99	1.02	0.74	1.25	1.81	0.25	0.57	1.41	0.51
	control	0.92	0.99	0.76	1.05	1.59	0.25	0.61	1.29	0.44
El Centro	Passive	1.43	1.38	0.45	1.68	1.34	0.39	1.19	1.46	0.56
	control	1.22	1.19	0.56	1.22	1.22	0.45	1.05	1.35	0.44
Rinaldi	Passive	1.05	1.04	0.77	1.20	2.13	0.28	0.82	1.71	0.52
	control	0.93	0.95	0.85	1.08	1.67	0.29	0.76	1.53	0.44
Kobe	Passive	1.12	1.43	0.62	1.69	1.78	0.35	0.70	1.54	0.50
	control	1.04	1.36	0.57	1.41	1.58	0.36	0.65	1.38	0.43
Jiji	Passive	0.81	0.82	0.67	0.98	1.38	0.18	0.58	1.43	0.46
	control	0.86	0.86	0.72	0.96	1.27	0.17	0.69	1.39	0.39
Erzinkan	Passive	1.04	1.07	0.74	1.16	1.66	0.25	0.68	1.28	0.52
	control	0.91	0.92	0.71	1.01	1.38	0.28	0.63	1.16	0.46

Table VI. Results for skyhook control (FP-y and FN-x).

Earthquake		J1	J2	J3	J4	J5	J6	J7	J8	J9
Newhall	Passive	1.02	1.06	0.70	1.36	1.64	0.30	0.61	1.44	0.51
	control	0.89	0.91	0.79	1.11	1.27	0.33	0.72	1.26	0.42
Sylmar	Passive	1.02	1.07	0.80	1.09	1.96	0.23	0.59	1.28	0.51
	control	0.94	1.00	0.77	0.92	1.56	0.25	0.58	1.17	0.45
El Centro	Passive	1.46	1.51	0.51	1.51	1.45	0.41	1.11	1.40	0.56
	control	1.43	1.21	0.77	1.15	1.21	0.38	0.97	1.27	0.43
Rinaldi	Passive	1.04	1.01	0.75	1.07	1.44	0.27	0.88	1.63	0.52
	control	0.91	0.90	0.85	1.00	1.36	0.29	0.80	1.66	0.44
Kobe	Passive	1.19	1.29	0.57	1.70	1.74	0.33	0.75	1.53	0.50
	control	1.08	1.14	0.51	1.25	1.49	0.33	0.76	1.37	0.42
Jiji	Passive	0.79	0.81	0.63	0.85	1.07	0.18	0.54	1.28	0.46
	control	0.86	0.86	0.70	0.89	0.98	0.17	0.67	1.13	0.39
Erzinkan	Passive	1.10	1.02	0.64	1.05	1.46	0.24	0.58	1.16	0.53
	control	0.96	0.95	0.61	1.00	1.58	0.26	0.53	1.04	0.47

The results of the active control of the benchmark problem with linear elastomeric isolation system are summarized in Tables I and II. Actuators are used apply the active control forces to the base of the structure. In this control strategy most of the response quantities are reduced substantially from the uncontrolled cases. The benefit of the active control strategy is the reduction of base displacements and shears of up to 25% without increase in drift or accelerations.

The results of clipped optimal control strategy for the benchmark problem with a linear elastomeric isolation system are presented in Tables III and IV. The semiactive force is applied to the base of the structure by sixteen MR dampers, eight in the X and eight in the Y direction. Fourteen of the MR dampers are located in the periphery of the base slab and two near the

Table VII. Results for corner drifts (normalized by uncontrolled values).

Earthquake		Active control	Clipped optimal	Skyhook control
Newhall	FP-x	0.85	1.28	1.10
	FN-x	0.81	1.11	1.03
Sylmar	FP-x	1.09	0.96	0.94
	FN-x	0.97	0.90	0.91
El Centro	FP-x	0.82	0.93	1.08
	FN-x	0.96	1.30	1.04
Rinaldi	FP-x	1.01	0.89	1.18
	FN-x	1.00	0.93	1.18
Kobe	FP-x	0.89	1.07	1.31
	FN-x	1.00	1.10	1.21
Jiji	FP-x	0.83	0.78	1.00
	FN-x	0.91	0.92	0.93
Erzinkan	FP-x	0.90	0.73	1.03
	FN-x	0.89	0.94	1.07

Table VIII. Linear isolation system uncontrolled response quantities (FP-x and FN-y).

	Newhall	Sylmar	El Centro	Rinaldi	Kobe	Jiji	Erzinkan
Peak base shear (normalized by W*)	0.180	0.272	0.098	0.238	0.171	0.488	0.250
Peak Str. Shear (normalized by W*)	0.150	0.228	0.084	0.207	0.143	0.408	0.204
Peak isolator deformation (m)	0.583	0.731	0.486	0.855	0.637	1.490	1.051
Peak IS drift (normalized by h*)	0.002	0.003	0.001	0.003	0.002	0.004	0.003
Peak absolute acceleration (g*)	0.231	0.318	0.135	0.329	0.191	0.509	0.267
RMS displacement (m)	0.281	0.297	0.201	0.333	0.264	0.344	0.471
RMS acceleration (g*)	0.074	0.098	0.055	0.098	0.082	0.100	0.131

*W: weight of structure (202 000 kN); h average storey height (4.04 m); g acceleration due to gravity (9.81 m/s^2).

Table IX. Linear isolation system uncontrolled response quantities (FP-y and FN-x).

	Newhall	Sylmar	El Centro	Rinaldi	Kobe	Jiji	Erzinkan
Peak base shear (normalized by W*)	0.200	0.314	0.096	0.258	0.142	0.557	0.287
Peak Str. shear (normalized by W*)	0.164	0.267	0.081	0.215	0.124	0.468	0.240
Peak isolator deformation (m)	0.593	0.763	0.325	0.791	0.602	1.549	0.955
Peak IS drift (normalized by h*)	0.003	0.004	0.001	0.003	0.002	0.006	0.003
Peak absolute acceleration (g*)	0.295	0.363	0.111	0.352	0.205	0.598	0.302
RMS displacement (m)	0.210	0.306	0.148	0.344	0.222	0.360	0.482
RMS acceleration (g*)	0.076	0.132	0.042	0.140	0.061	0.126	0.178

*W: weight of structure (202 000 kN); h average storey height (4.04 m); g acceleration due to gravity (9.81 m/s^2).

center of mass of the base slab. Performance indices are presented in Tables III and IV for both passive and semiactive control cases. The advantage of semiactive clipped optimal control is evident in significant reductions in base displacements as compared to the active control case.

Table X. Linear isolation system with friction uncontrolled response quantities (FP-x and FN-y).

	Newhall	Sylmar	El Centro	Rinaldi	Kobe	Jiji	Erzinkan
Peak base shear (normalized by W*)	0.170	0.245	0.083	0.228	0.140	0.424	0.220
Peak Str. shear (normalized by W*)	0.151	0.213	0.086	0.199	0.110	0.352	0.180
Peak isolator deformation (m)	0.300	0.489	0.108	0.433	0.252	1.095	0.512
Peak IS drift (normalized by h*)	0.002	0.003	0.002	0.003	0.002	0.004	0.003
Peak absolute acceleration (g*)	0.572	0.355	0.402	0.338	0.360	0.478	0.270
RMS displacement (m)	0.071	0.124	0.023	0.084	0.050	0.166	0.151
RMS acceleration (g*)	0.080	0.076	0.079	0.071	0.083	0.071	0.074

*W: weight of structure (202 000 kN); h average storey height (4.04 m); g acceleration due to gravity (9.81 m/s^2).

Table XI. Linear isolation system with friction uncontrolled response quantities (FP-y and FN-x).

	Newhall	Sylmar	El Centro	Rinaldi	Kobe	Jiji	Erzinkan
Peak base shear (normalized by W*)	0.177	0.251	0.080	0.232	0.140	0.428	0.225
Peak Str. shear (normalized by W*)	0.162	0.205	0.087	0.201	0.119	0.363	0.195
Peak isolator deformation (m)	0.292	0.495	0.085	0.428	0.281	1.188	0.563
Peak IS drift (normalized by h*)	0.003	0.003	0.002	0.003	0.002	0.005	0.003
Peak absolute acceleration (g*)	0.464	0.434	0.375	0.377	0.368	0.493	0.319
RMS displacement (m)	0.068	0.133	0.020	0.084	0.051	0.182	0.168
RMS acceleration (g*)	0.081	0.079	0.079	0.068	0.082	0.076	0.082

*W: weight of structure (202 000 kN); h average storey height (4.04 m); g acceleration due to gravity (9.81 m/s^2).

The reduction in base displacements is about 25–50% compared with 10–25% for the active case. The reductions are achieved at the cost of increased floor accelerations and inter-storey drifts; however, the increases in the semiactive control case are less than that of the passive damping case. This increase is observed mostly at higher floors. The performance of controlled case is better than the passive case in terms of achieving the good reduction in base drifts with a correspondingly lower increase in floor accelerations and storey drifts. It is worth noting that the sample controllers presented are not meant to be competitive and hence, further reductions are possible even for base displacements in the semiactive control case with better control algorithms.

The results of the skyhook control algorithm for the benchmark problem with friction are presented in Tables V and VI. Performance indices are presented in Tables V and VI for both the passive and skyhook control cases. The skyhook controller performs better than the passive case in all earthquakes. The base and structural shear remains at the level of uncontrolled structure for all earthquakes except El Centro and Kobe for the controlled case. There is an increase in the base and structure shear for El Centro and Kobe earthquakes. The reduction in maximum base displacements is 15–50%. The results of the passive case are better than the controlled case for peak base displacements in most cases; however, the inter-storey drifts in the controlled case are significantly better than the passive case. For both the passive and controlled cases, the inter-storey drifts are higher than in the uncontrolled case. The peak accelerations increased for both controlled and passive cases with

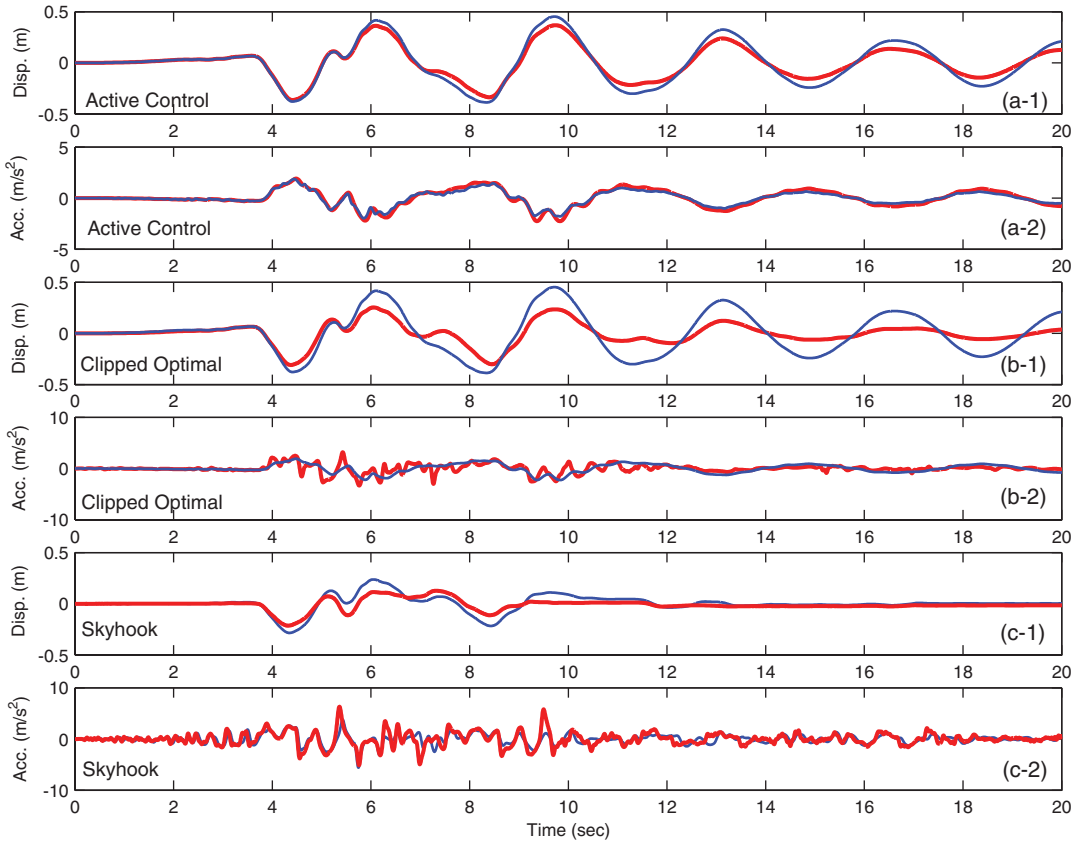

Figure 5. Time-history responses, both controlled (gray, thick) and uncontrolled (black, thin), at the center of mass of the base in the NS direction for the Newhall earthquake FN-x and FP-y components acting on the benchmark building: (a-1,a-2) Base displacement and top floor acceleration responses for active control, linear elastomeric system; (b-1,b-2) Base displacement and top floor acceleration responses for clipped optimal control, linear elastomeric system; (c-1,c-2) Base displacement and top floor acceleration responses for skyhook control, friction isolation system.

the magnitude of increase much higher for the passive case in all excitations. It is worth noting that further reductions are possible in the semiactive control case with better control algorithms.

7. NOTE ON PHASE II

In phase II the participants can compare the results of their controllers with the sample controllers presented by Nagarajaiah and Narasimhan [35] for nonlinear friction isolation system and/or the sample controller presented by Erkus and Johnson [36] for bilinear elastomeric isolation system such as lead–rubber isolation systems.

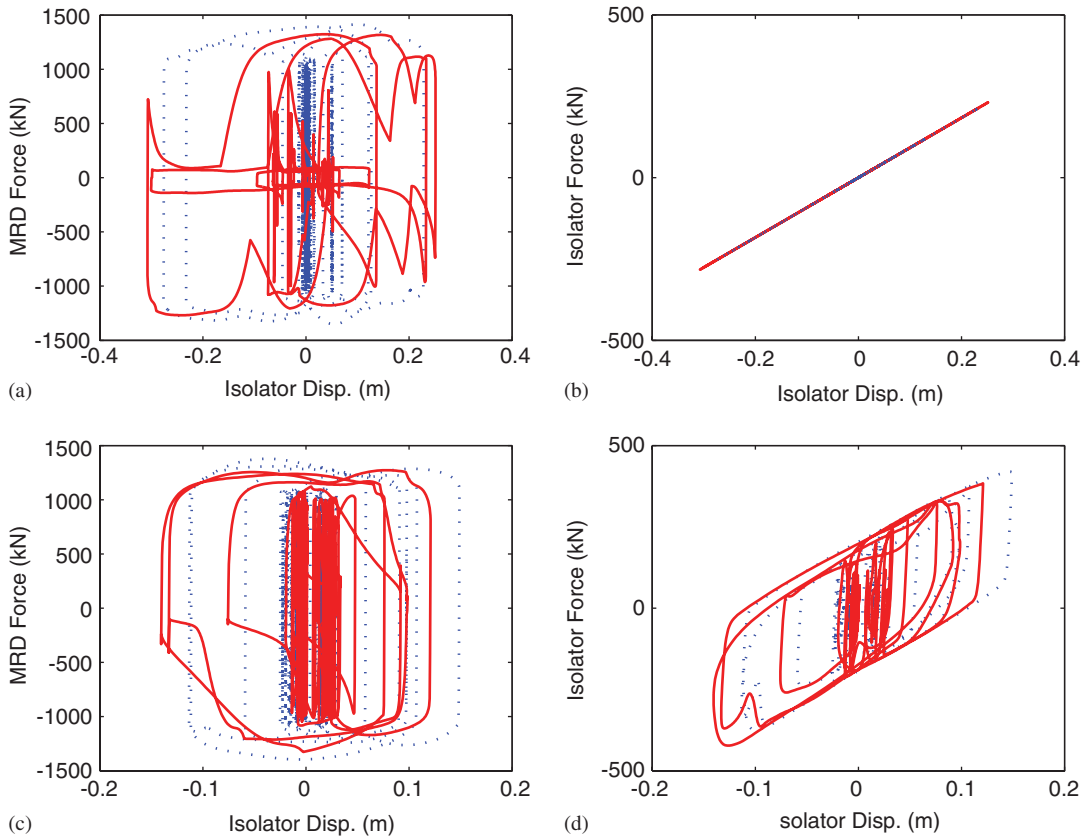

Figure 6. (a) Clipped optimal MR damper force–displacement for Newhall—y-direction; (b) clipped optimal linear bearing force–displacement for Newhall—y-direction; (c) Skyhook MR damper force–displacement for Kobe y-direction; (d) Skyhook frictional force–displacement for Kobe y-direction. Both passive-on (black, dashed) and controlled (gray, solid) are shown; earthquake FP-x and FN-y and the bearing and device location near the center of mass of the base.

8. CONCLUDING REMARKS

In phase I, the participants can compare the results of their controllers with the results of the sample active and semiactive controllers presented in this paper for the nominal linear isolation system. Additionally, they can also compare the results of their controllers with a preliminary skyhook controller presented in this paper. The control algorithms presented in this paper are for illustration and design purposes only and are not meant to be competitive. The models and data for the base isolated benchmark problem are available in a set of MATLAB m-files and C executables. They can be accessed from *http://www.ruf.rice.edu/~nagaraja/baseisolationbenchmark.htm*.

ACKNOWLEDGEMENTS

Partial funding provided by the National Science Foundation, NSF-CAREER Grant 9996290 is gratefully acknowledged. The authors would like to thank Professor Bill Spencer, University of Illinois at Urbana-Champaign for his suggestions.

REFERENCES

1. Reinhorn A, Soong T, Wen CY. Base-isolated structures with active control. *Proceedings of the ASME PVP Conference*, vol. PVP-127, ASME, San Diego, CA, 1987; 413–420.
2. Nagarajaiah S, Riley MA, Reinhorn A. Control of sliding-isolated bridge with absolute acceleration feedback. *Journal of Engineering Mechanics* (ASCE) 1993; **119**(11):2317–2332.
3. Nagarajaiah S. Fuzzy controller for structures with hybrid isolation system. *Proceedings of the 1st World Conference on Structural Control*, vol. TA2, Los Angeles, CA, 1994; 67–76.
4. Reinhorn A, Riley M. Control of bridge vibrations with hybrid devices. *Proceedings of the 1st World Conference on Structural Control*, vol. TA2, Los Angeles, CA, 1994; 50–59.
5. Yoshida K, Kang S, Kim T. LQG control and H_∞ control of vibration isolation for MDOF systems. *Proceedings of the 1st World Conference on Structural Control*, vol. TA4, Los Angeles, CA, 1994; 43–52.
6. Yang J, Wu J, Agrawal A. Sliding mode control of nonlinear and hysteretic structures. *Journal of Engineering Mechanics* (ASCE) 1995; **121**(12):1386–1390.
7. Yang J, Wu J, Reinhorn A, Riley M. Control of sliding-isolated buildings using sliding-mode control. *Journal of Structural Engineering* (ASCE) 1996; **122**:179–186.
8. Yang J, Agrawal A. Semiactive hybrid control systems for nonlinear buildings against near-field earthquakes. *Journal of Engineering Structures* 2002; **24**:271–280.
9. Symans MD, Kelly SW. Fuzzy logic control of bridge structures using intelligent semi-active seismic isolation. *Earthquake Engineering and Structural Dynamics* 1999; **28**:37–60.
10. Yoshida K, Yoshida S, Takeda Y. Semi-active control of base isolation using feedforward information of disturbance. *Proceedings of the 2nd World Conference on Structural Control*, vol. 1, Kyoto, Japan, 1999; 377–386.
11. Nagarajaiah S, Sahasrabudhe S, Iyer R. Seismic response of sliding isolated bridges with MR dampers. *Proceedings of the American Control Conference*, 2000; CDROM.
12. Spencer BF, Johnson EA, Ramallo JC. Smart isolation for seismic control. *JSME International Journal*, *Series C* 2000; **43**(3):704–711.
13. Sahasrabudhe S, Nagarajaiah S, Hard C. Experimental study of sliding isolated bridges with smart dampers subjected to near source ground motion. *Proceedings of the 13th Engineering Mechanics Conference*, Austin, Texas, 2000; CDROM.
14. Ramallo J, Johnson EA, Spencer B. Smart base isolation systems. *Journal of Engineering Mechanics* (ASCE) 2002; **128**(10):1088–1099.
15. Madden G, Wongprasert N, Symans MD. Analytical and numerical study of a smart base isolation system for seismic protection of buildings. *Computer Aided Civil Infrastructural Engineering* 2003; **18**:19–30.
16. Caughey TK. The benchmark problem. *Earthquake Engineering and Structural Dynamics* 1998; **27**(11):1125.
17. Spencer BF, Dyke SJ, Deoskar HS. Benchmark problems in structural control. Part 1—active mass driver system. *Earthquake Engineering and Structural Dynamics* 1998; **27**(11):1127–1139.
18. Spencer BF, Dyke SJ, Deoskar HS. Benchmark problems in structural control. Part 2—active tendon system. *Earthquake Engineering and Structural Dynamics* 1998b; **27**(11):1141–1147.
19. Ohtori Y, Christenson RE, Spencer BF, Dyke SJ. Benchmark problems in seismically excited nonlinear buildings. *Journal of Engineering Mechanics* (ASCE) 2004; **130**(4):366–385.
20. Yang J, Agrawal A, Samali B, Wu JC. A benchmark problem for response control of wind excited tall buildings. *Journal of Engineering Mechanics* (ASCE) 2004; **130**(4):437–446.
21. Dyke SJ, Caicedo JM, Turan G, Bergman LA, Hague S. Phase 1: benchmark control problem for seismic response of cable-stayed bridges. *Journal of Structural Engineering* (ASCE) 2003; **129**(7):857–872.
22. Narasimhan S, Nagarajaiah S, Johnson EA, Gavin HP. Benchmark problem for control of base isolated buildings. *Proceedings of the 3rd World Conference on Structural Control*, Como, Italy, 2002; CDROM.
23. Narasimhan S, Nagarajaiah S, Johnson EA, Gavin HP. Smart base isolated building benchmark problem. *Proceedings of the 16th Engineering Mechanics Conference*, ASCE, University of Washington, 2003; CDROM.
24. Narasimhan S, Nagarajaiah S, Johnson EA, Gavin HP. Smart base isolated benchmark building part I: problem definition. *Proceedings of the 4th International Workshop on Structural Control and Health Monitoring*, Columbia University, June 10–11, 2004; CDROM.
25. Narasimhan S, Nagarajaiah S, Johnson EA, Gavin HP. Smart base isolated benchmark building part I: problem definition. *Journal of Structural Control and Health Monitoring* 2005, in review.

26. Nagarajaiah S, Narasimhan S. Controllers for benchmark base isolated building with linear and friction isolation system. *Proceedings of the 16th Engineering Mechanics Conference*, ASCE, University of Washington, 2003; CDROM.
27. Nagarajaiah S, Narasimhan S. Phase I: controllers for benchmark base isolated building. Part I. *Proceedings of the 4th International Workshop on Structural Control and Health Monitoring*, Columbia University, 10–11 June, 2004.
28. Dyke SJ, Spencer BF, Sain MK, Carlson JD. Seismic response reduction using magnetorheological dampers. *Proceedings of the IFAC World Congress*, vol. L, San Francisco, California, 30 June – 5 July, 1996; 145–150.
29. Karnopp D, Crosby MJ, Harwood RA. Vibration control using semi-active force generators. *Journal of Engineering for Industry* (ASME) 1974; **96**(2):619–626.
30. Yoshioka H, Ramallo JC, Spencer BF. Smart base isolation systems employing magnetorheological dampers. *Journal of Engineering Mechanics* (ASCE) 2002; **128**(5):540–551.
31. Davison EJ. A method for simplifying linear dynamic systems. *IEEE Transactions on Automatic Control* 1966; **AC-11**(1):93–101.
32. Agrawal A, Xu Z. A novel active controller design based on H_2/LQG algorithm with pulse filters. *Proceedings of the 4th International Workshop on Structural Control and Health Monitoring*, Columbia University, 10–11 June, 2004.
33. Spencer BF, Dyke SJ, Sain MK, Carlson JD. Phenomenological model of a magnetorheological damper. *Journal of Engineering Mechanics* 1997; **123**(3):230–238.
34. Carlson JD, Charzan MJ. Magnetorheological fluid dampers. *U.S. Patent No. 5,277,281*, 1994.
35. Nagarajaiah S, Narasimhan S. Smart base isolated benchmark building phase II. Part IV sample controllers for nonlinear friction isolation system. www.ruf.rice.edu/∼nagaraja/baseisolationbenchmark.htm
36. Erkus B, Johnson EA. Smart base isolated benchmark building part III: phase II sample controller for bilinear isolation. *Journal of Structural Control and Health Monitoring* 2006.
37. Makris N. Rigidity-plasticity-viscocity: can electrorheological dampers protect base-isolated structures from near-source earthquakes. *Earthquake Engineering and Structural Dynamics* 1997; **26**:571–591.
38. MATLAB. The Math Works, Inc., 2000.
39. Nagarajaiah S, Reinhorn AM, Constantinou MC. Nonlinear dynamic analysis of 3-d-base-isolated structures. *Journal of Structural Engineering* (ASCE) 1991a; **117**(7):2035–2054.
40. Nagarajaiah S, Reinhorn AM, Constantinou MC. 3D-BASIS: nonlinear dynamic analysis of three dimensional base isolated structures—part 2. *Report No. NCEER-91-0005*, National Center for Earthquake Engineering Research, State University of New York, Buffalo, 1991b.
41. Nagarajaiah S, Sun X. Response of base-isolated USC hospital building in northridge earthquake. *Journal of Structural Engineering* (ASCE) 2000; **126**(10):1177–1186.
42. Stengel R. *Optimal Control and Estimation*. Dover Publications: New York, 1994.
43. Yang J, Wu J, Kawashima K, Unjoh S. Hybrid control of seismic-excited bridge structures. *Earthquake Engineering and Structural Dynamics* 1995; **24**(11):1437–1451.

